TIMING AND MOVEMENT OF THE EGIIN DAVAA FAULT, HANGAY MOUNTAINS, MONGOLIA

EMILY PARKER, Colorado College
Sponsor: Eric Leonard
JULIANA WILLIAMS, Whitman College
Sponsor: Kevin Pogue
UYANGA BOLD, Mongolian University of Science and Technology
ERDENEBAYAR OYUN, Mongolian University of Science and Technology
Sponsor: A. Bayasgalan

INTRODUCTION

This study is focused on the Egiin Davaa Fault (EDF), a major range-bounding normal fault in the southeastern part of the Hangay Dome in Central Mongolia. Only three previous studies (Khilko et al., 1985; Baljinnyam et al., 1993 Cunningham, 2001) mention the EDF. Khilko et al. (1985) propose that the last rupture along this fault occurred between 300 and 500 years ago, based on observed steep-walled tension gashes. Fault motion has been described as both right-lateral oblique (Cunningham, 2001) and left-lateral oblique (Baljinnyam et al., 1993).

The goals for this project are to provide detailed and quantitative estimations of along-strike variations in geometry, fault age, amount of throw, sense of motion, and the timing of the most recent rupture. The age of recent fault rupture was investigated via radiocarbon dating of key horizons from paleoseismic trenches along with slope-diffusion modeling of the fault scarp. Fault sense of motion was analyzed through slickenline measurements and investigation of the displacement of alluvial fan axes.

TECTONIC SETTING

The Hangay region is a 200,000 km2 zone of upwarping and moderate extension. Maximum elevations exceed 4021 m. Cunningham (2001) asserts that Oligocene sedimentary deposits and volcanics are tilted and raised, indicating that high elevations have been attained only in the last 25Ma. Although areas of high elevation are typically associated with compressional tectonic activity, the Hangay is characterized by extensional faulting within a larger actively deforming setting (Bayasgalan et al., 2005). The major tectonic stresses in the region are those generated by the Indian-Eurasian collision, 2,000 to 3,000 km south-southwest of Mongolia (Tapponnier and Molnar, 1979). Baljinnyam et al. (1993) propose that Mongolia is simultaneously undergoing northeast-southwest shortening and northwest-southeast extension. GPS measurements indicate that India is moving northeast relative to Eurasia at a rate of 4 cm/yr (Calais et al., 2003). This northeast-southwest compressive stress has caused extensive and complex deformation, producing such geographic features as the Mongolian and Gobi Altai ranges, large continental-scale strike-slip faults such as the Bulnay, and potentially the Baikal Rift in Russia (Tapponnier and Molnar, 1979). These features are at the expected orientations for northeast-southwest compressive stress, while the extension in the Hangay is not. Within the Hangay Dome, normal faults have varying orientations, rather than one dominant orientation (Cunningham, 2001). In the case of the EDF, its strike of N61° E is roughly parallel to the direction of the compressional stress from the Indian-Eurasian collision.

DESCRIPTION OF FAULT
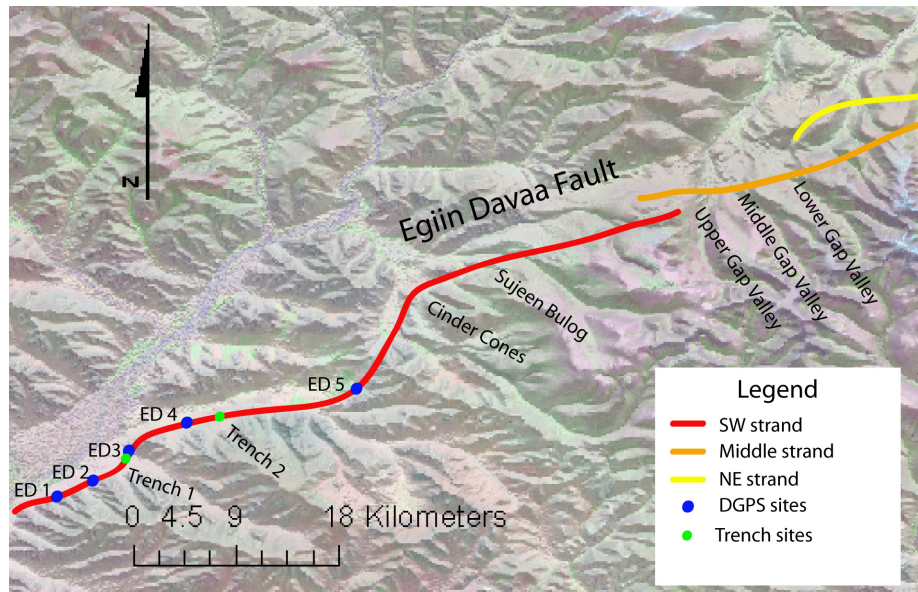
Figure 1. Map of the EDF, showing the three strands and Differential GPS and Trench sites.

The EDF crosses a major drainage divide in the Hangay Mountains, north of which rivers drain to the Arctic, and south of which rivers flow to the internally-drained Valley of Lakes – Gobi. The EDF strikes roughly N61° E with an average dip at the surface of 43° NW (Fig. 1). The fault consists of three primary strands, which we will describe from southwest to northeast. The last rupture produced an earthquake scarp along the southwestern and possibly the middle strands (Fig. 1). Our efforts focused primarily upon the 51-km-long southwestern strand. This strand is the most recently active based upon fault-scarp morphology and can be subdivided into six segments based upon the segment strike orientation and rupture characteristics, although only five segments ruptured during the last earthquake as determined by field observations and from satellite imagery. The three longer segments strike at N61°E and alternate with three shorter segments striking at N15°E (Fig. 1). The earthquake scarp is much lower along the shorter N15°E segments.   Bedrock is exposed very rarely on the scarp. Along most of its length the scarp cuts unconsolidated alluvium. The fault scarp ranges from 2 to 5 m high. In some places a shallow half-graben is visible at the base of the scarp, which is discernible as patches of darker grass produced by the collection of water in areas of low topography (Fig. 2).

 Figure 2. Photograph of scarp on southeastern segment, with darker patches of grass at the base.

At the west end of the northernmost segment of the southwestern strand, the fault cuts the edge of a Quaternary cinder cone (47.10º N, 99.69º E). The cone is part of a chain of Quaternary cinder cones (Eckstrand and Enkhbaatar, this volume) that intersects a bend in the fault and, based on its proximity to the fault, may have resulted from magma ascension along the EDF. West of the cinder cones, along one of the N15ºE segments, the scarp appears to step left several times on a small scale. The fault plane is exposed on the quartzite footwall along this segment at Suujiin Bulag spring (Fig. 3). Spring activity and erosion of the regolith on

the downthrown block have exaggerated the apparent displacement of the scarp.

are no clearly identifiable earthquake scarps along this strand. The northeastern strand is

Figure 3. a. Footwall outcrop at Suujiin Bulog. b. Slickenlines on outcrop.

The middle strand of the fault consists of only one segment, and is moderately dissected by streams and previous glacial activity. This strand primarily cuts Oligocene basalt flows, however the underlying metamorphic rock and granite are exposed near Chuluut Gol. Pleistocene glaciation produced bedrock-cored moraines in this area. These moraines have been vertically offset approximately 7 meters by the fault. In most locations along the middle strand, the fault cuts through basalt (covered by a thin layer of colluvium) rather than unconsolidated sediments, so it is difficult to compare the degree of degradation between this strand and the one to the southwest. However there are small intermittent scarps exposed in drift in Middle Gap Valley and Lower Gap Valley, including a double scarp in Middle Gap Valley. These scarps are not as distinct as the scarps on the southwest strand. The fault plane is exposed on the footwall in Middle Gap Valley, and has an orientation of N70°E, 43°NW. We also measured an orientation of N48°E, 44°NW, at a different location along this segment by tracing the fault through a valley and using a three-point solution (47.21ºN, 100.03ºE).

The northeastern strand has the greatest amount of total displacement and is the most dissected by streams and previous glacial activity. There

likely the least recently active strand of the EDF based on the absence of recent scarps and the degree of dissection. This strand is located in an area that was glaciated during the late Pleistocene and as a result, the surface expression of the fault is subdued. The glacial deposits are not cut by the fault, indicating that this strand has been inactive since the last glaciation in this area.

METHODS

The southwestern and middle strands were surveyed on foot in order to better define the nature and extent of the fault scarp. Fault scarp profiles were created by differential GPS at Suujiin Bulag and by tape at Middle Gap Valley. Two paleoseismic trenches were dug across the scarp, Trench S at 46.97ºN 99.45ºE and Trench N at 47.00ºN 99.53ºE. These two trenches were located on segments of the fault with different strikes, to account for variation in orientation and displacement. Trenches were dug crossing the scarp to construct trench logs, to determine if the scarp was produced by one event, and to learn the age of the last event. Charcoal was discovered in Trench S (Sample A), which was collected along with soil samples (B and C) for radiocarbon analysis (Fig. 4 and 5). Following the conventions of Stuiver and Polach (1977),

the radiocarbon ages were converted to calibrated years using online CalPal calibration program (May 2006).

Differential GPS surveys were conducted at five locations on the southwestern strand of the fault; they are designated ED1 to ED5 from southwest to northeast. Rigurel Surveys ED1 and ED2 are located on the same segment. ED3 is on a short, N15°E segment. This survey site was also the location of Trench S. Trench N is located to the east of survey ED4 (99.54°E, 47.00°N) on the same segment. Survey ED5 is located on a large bend in the fault. At sites ED3 and ED5 we surveyed only a few profiles. Digital elevation models (DEMs) were created from the differential GPS survey data, which were used to create scarp-parallel profiles above and below the scarp. Comparison of topographic features in these profiles allows for the quantification of lateral slip on the scarp.

The differential GPS data was also used to create scarp-perpendicular profiles. The shapes of these profiles can provide additional insight into the age of the scarp. A scarp in unconsolidated materials should degrade according to the standard slope diffusion equation (Colman and Watson, 1983; Hanks, 2000). The diffusion equation states that the change in relative elevation u of any point with respect to time t is equal to the mass diffusivity constant $\varkappa$ to the curvature of the scarp at that

point $\frac{\partial^2 u}{\partial x^2}$. Relative elevation u is a function of cross strike horizontal position x and time t, $u(x, t)$. The mass diffusivity constant u is controlled by environmental factors such as scarp material, climate and vegetation.

$$\frac{\partial u}{\partial t} = \kappa \frac{\partial^2 u}{\partial x^2} \qquad \text{(eq. 1)}$$

The equation from Avouac (1993) (eq. 2) was used to create modeled profiles

$$\frac{\partial u}{\partial x} = \frac{2a}{\sqrt{\pi \tau}} e^{-\frac{x^2}{4\tau}} + b \qquad \text{(eq. 2)}$$

where $\frac{\delta u}{\delta x}$ is the slope of the scarp at point x along the profile perpendicular to strike, 2a is the throw of the scarp, b is the initial slope of the surrounding topography, and τ is the diffusion age, a measure of scarp degradation that can be related to age through the equation,

$$\tau = \varkappa t \qquad \text{(eq. 3)}$$

The slopes of our measured profiles were fit to this model by changing the value of τ and minimizing the sum of the squares of the differences between the modeled and measured values. This method provides a diffusion age τ of the scarp rather than an absolute age. However by using the age determined by radiocarbon dating as the true age t we can get a mass diffusivity constant $\varkappa$ from the relationship

$$x. \quad \frac{\tau}{t} = \kappa \quad \text{equation 3}$$

The diffusivity constant can then be compared to diffusivity constants for similar areas of Holocene extensional faulting.

RESULTS AND DISCUSSION

Trench S Log Description and Interpretation
Trench S (Fig. 4) was 14 m long and over 2 m at the deepest point. The trench was dug across the fault scarp on an alluvial fan. The scarp shows approximately 3 m of vertical offset at this location. The clasts in the fan are primarily tabular cobbles derived from the uplifted metasedimentary bedrock. Silt and sand lenses were deposited within the alluvium, likely due to shifting active alluvial channels. The earthquake produced a fissure approximately 2.5 meters deep, which filled with colluvium. A lens of alluvium is interpreted to have fallen into the fissure before the fissure entirely filled with colluvium. The reversed imbrication of the clasts suggests that the alluvium fell into the fissure as a coherent block, and thus predates the rupture. However, absolute dating on this alluvium was not possible, so it could not be
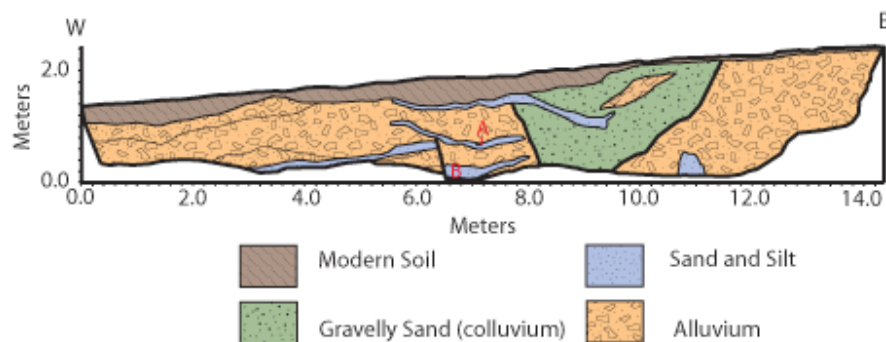
Figure 4. Log of Trench S showing sedimentary units and locations of samples A and B.

used to date the rupture. We believe the alluvial fan ceased being active before the most recent earthquake occurred, evidenced by the fact that only the modern soil was deposited over the infilled fissure. The modern soil is composed of a 10-cm thick layer of organics, loess and occasional clasts.

Trench N Log Description and Interpretation
Trench N (Fig. 5) was 8.5 m long and over 2 m at the deepest point. This trench did not cross the plane of the fault; due to time constraints we could not lengthen the trench. The section exposed by this trench is similar to that of meters 6 - 9 in Trench S. The scarp shows approximately 2.5 m of vertical offset here. Only the downthrown block and part of the scarp-parallel graben produced by the earthquake are visible in the trench. The fissure was partly filled with sand and silt, presumably deposited by fluvial and/or eolian processes. This fine-grained sediment forms a 1-m-thick deposit, above which coarse, non-imbricated, cobble-dominated colluvium filled the rest of the fissure.

Radiocarbon Dates and Interpretation
Sample B, collected from a sand lens in Trench S, yielded a calibrated date of 7,673 ± 35 years BP; sample A, collected from a stratigraphically higher sand lens in Trench S, yielded a calibrated date of 7,369 ± 35 years BP; sample C, collected from the silty-sand unit in Trench N, yielded a calibrated date of 4,916 ±38 years BP. Samples A and B were collected from sediments that are stratigraphically lower than the fissure sediments, and are therefore interpreted to predate the rupture. Sample C was collected from the silty-sand that is interpreted to be the first sediment deposited into the fissure after the rupture. Sample C is interpreted to post-date the rupture. Given that time would elapse before the sediment filled the rupture, the earthquake would have occurred just before the date yielded by sample C. Thus the ages of samples A and C constrain the date of the rupture. Therefore, the interpreted date of the last rupture is between 7,369 ± 35 and 4,916 ± 38 years BP, most likely about 5,000 years BP.
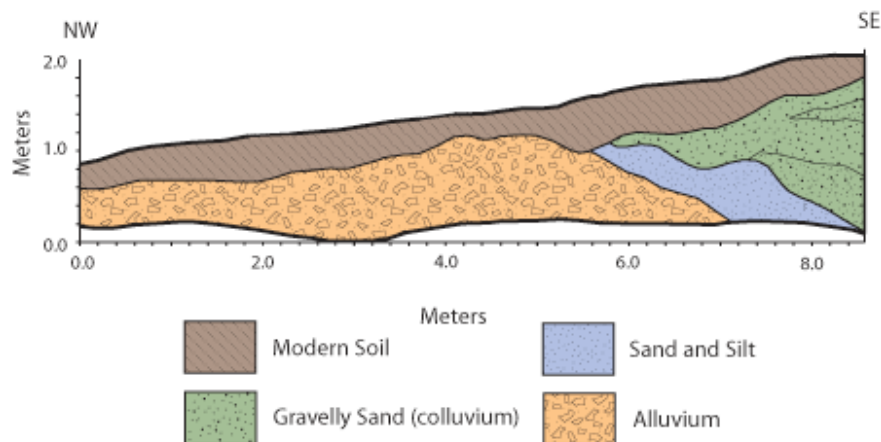
Figure 5. Log of Trench N showing sedimentary units and location of sample C.

The primary source of error in this analysis is our interpretation of the trench logs. If the layers from which the samples were collected do not actually pre- and post-date the earthquake, these dates would be invalid constraints on the date of the last rupture. Khilko et al. (1985) who proposed that the fault ruptured 300-500 years BP, based on the morphology of steep-walled tension gashes. However, we saw no evidence in the field of tension gashes. The radiocarbon analyses, combined with the lack of tension gashes, seem to disprove the date proposed by Khilko et al. (1985). Oral history tells of a major earthquake in this area of the Hangay Dome approximately 300 years ago, but it could have been produced by the Ar Hotol Fault, or another yet unidentified fault, rather than the Egiin Davaa Fault.

Degradation Modeling

Fitting of modeled scarp profiles (Fig. 6) gives an average diffusion age τ of 41.5 m^2 with a standard deviation of 24 ± 14 m^2. Based on our age of 7369 ± 35 to 4916 ± 38 years BP for the scarp determined by radiocarbon dating, the mass diffusivity constant $\varkappa$ for the Egiin Davaa scarp is 6.8 ± 2.9.
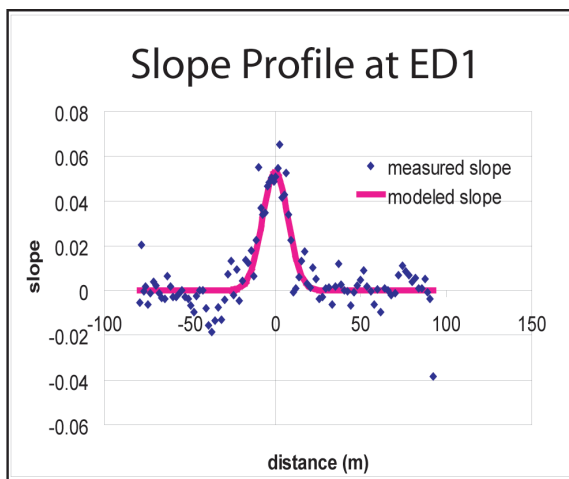
Figure 6. Example of a modeled slope profile from ED 1.

A table of previously calculated mass diffusivity constants can be found in Table 2 of Hanks (2000). The mass diffusivity constant calculated for the Egiin Davaa scarp, 6.8 ± 2.9 is higher than most of the values listed in this table, with the exception of those in California. This suggests that the Hangay region has a very rapidly eroding environment, which does not seem to be the case based on knowledge of the local climate. However, there are three possible sources of error that could contribute to an erroneously high mass diffusivity constant. The first possibility is that there is error in the radiocarbon date, as noted above. If we assume that the diffusion age is accurate, then the true age of the scarp t would have to be greater to produce a lower mass diffusivity constant. More likely sources of error may exist in the diffusion age τ. Modeling the degradation of a scarp by the diffusion equation may be an oversimplification of the actual processes at work. The linear relationship between the diffusion age τ and time t, $\tau = \varkappa t$ is an assumption that may not be accurate. Field measurement errors could also contribute to error in the diffusion age. However the precision of the differential GPS is within a few millimeters, so this error is probably very small.

Lateral Motion

Data from the bedrock outcrop at Suujiin Bulag indicate that the mean trend and plunge of slickenlines is N31°E, 35.7° with a rake of 45° NE (Fig.7). Assuming a component of normal motion, the striae at Suujiin Bulag are indicative of right lateral oblique motion. Such motion would require about 6 m of lateral displacement to produce a 4-m-high scarp on a fault dipping 43°.
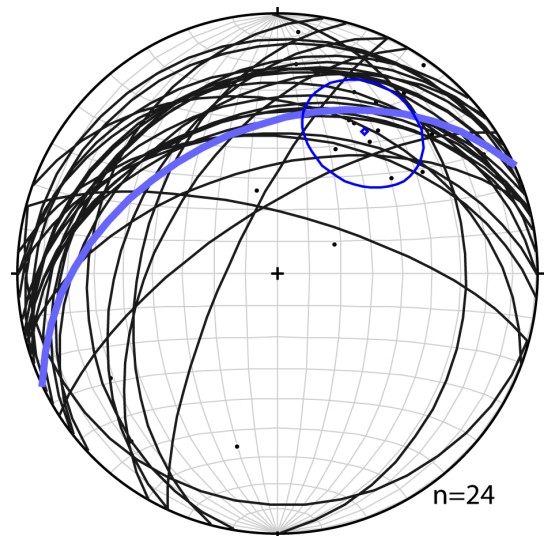
Figure 7. Equal Area Stereonet showing measured surfaces at Suujiin Bulag with fault surface and mean vector solution for slickenlines.

The scarp-parallel profiles at site ED2 have topographical features that are clearly identifiable above and below the scarp. (Fig. 8) These features are in line across the scarp, showing no apparent strike-parallel displacement. However, on the scale of the features we observed in the field such as alluvial fans, a 6 m lateral displacement may have been difficult to detect. The slickenlines and polished surfaces at Suujeen Bulog are on crystalline bedrock, which is juxtaposed against basin sediments. This implies that the striae were produced before the most recent earthquake. It is possible that the sense of movement of the Egiin Daava fault has changed through time or that the lineations measured on the bedrock outcrop at Buujeen Bulog were inherited from older tectonic events.

$$M = 6.61 \pm 0.09 + 0.71 \pm 0.15 * \log(MD) \quad \text{(eq. 4)}$$
$$M = 6.78 \pm 0.12 + 0.65 \pm 0.25 * \log(AD) \quad \text{(eq. 5)}$$
$$M = 4.86 \pm 0.34 + 1.32 \pm 0.26 * \log(SRL) \quad \text{(eq. 6)}$$

Table 1 shows the magnitudes calculated from these relationships. Displacements are determined from scarp height measurements assuming that the dip of the fault is 43° and that the slip direction is 45° from the dip, as indicated by slickenlines. Because both the southwestern and middle strands have scarps, we are uncertain whether the middle stand ruptured in the same event or in an older one. The middle strand scarp seems older but because the scarp material is different it is difficult to say for sure. Structural
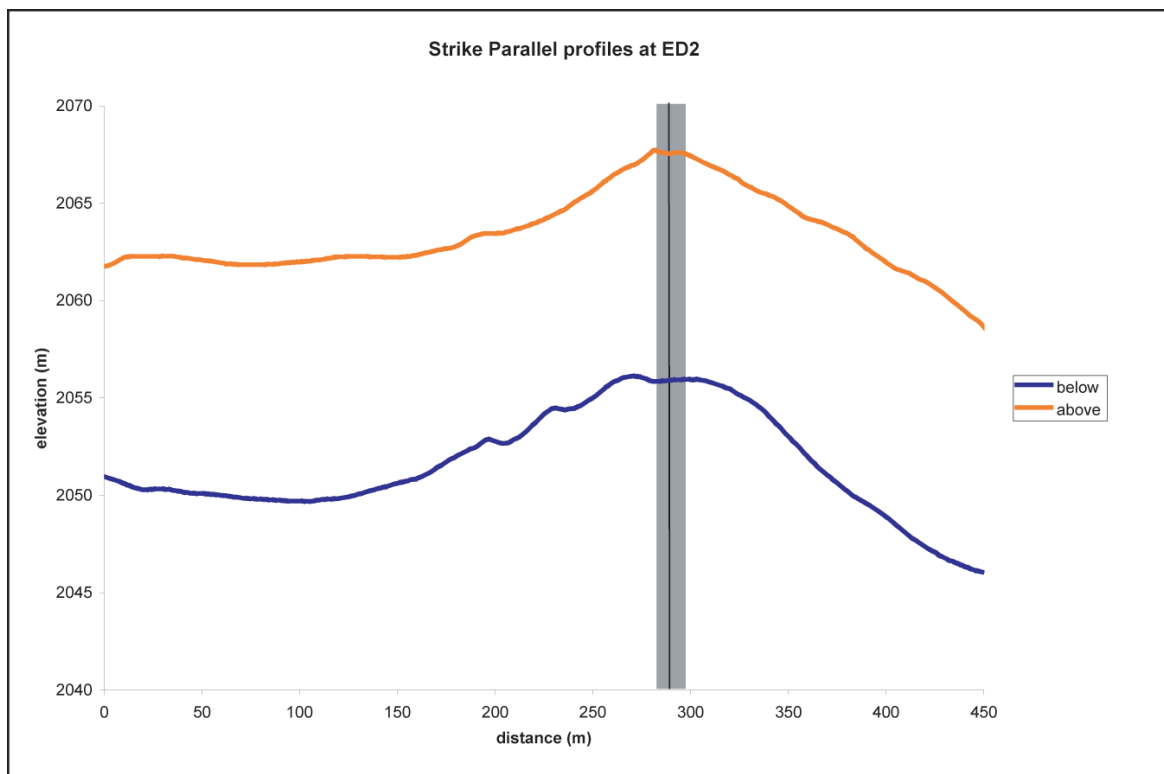
Figure 8. (Above) Scarp parallel profiles showing fan crest at ED2 above and below the scarp. Gray area shows 6-m margin on either side of the fan crest.

Magnitude
The relationships for Moment Magnitude M, surface rupture length SRL, maximum displacement MD, and average displacement AD as derived by Wells and Coppersmith (1994) are shown in equations 4–6.

discontinuities such as en echelon steps usually are also boundaries for earthquake ruptures, however earthquakes of magnitude greater than 7 have been recorded to rupture across segment boundaries (Yeats et al., 1997).   The magnitude was estimated from surface rupture length by both including and excluding the middle segment.

Table 1. Magnitudes calculated from eq. 4-6 and associated Range

Determining Factor	Value	Magnitude	Range
max displacement (oblique)	12 m	7.4	7.1-7.6
mean displacement (oblique)	7 m	7.3	7.0-7.7
rupture length (SW strand only)	51 km	7.1	6.3-7.9
rupture length (SW and middle strands)	70 km	7.3	6.5-8.1

There are many assumptions that go into the calculations of the magnitude. The most obvious of these assumptions is that the scarp was produced in a single earthquake event. A multiple event scarp can be identified if the events are significantly different in age. Two events separated by even hundreds of years would not be significantly evident in 6 ka of erosion, however a multiple event scarp could be very significant in the implications of the magnitude. There is no evidence in the trenches of multiple events. We did not measure the height of the scarp in many locations, therefore our estimations of the maximum and average scarp height may be inaccurate. Calculated magnitudes (Table 1) based on the surface rupture length with and without the middle segment contain the magnitudes calculated from the displacement in their errors. It is therefore difficult to say based on these relationships whether the two scarps were formed in a single event. Based on observations of the scarps along the southwestern and middle strands, it seems unlikely that they formed in a single event but the possibility needs more investigation.

CONCLUSION

Khilko et al. (1985) suggested a date for the last rupture along the Egiin Davaa Fault of 300-500 years ago. Their assessment was based on qualitative analysis of the degradation of the scarp, in particular an interpretation of steep-walled tension gashes. We found that the age of the last rupture is between 7,369 ± 35 and 4,916 ± 38 years BP based on radiocarbon dating. This date is significantly older than the date proposed by Khilko et al. (1985). These radiocarbon dates may represent the penultimate earthquake; however a quantitative study of the degradation of the scarp suggests that, if anything, the scarp has degraded further than would be expected for the radiocarbon age.

There has been some dispute in the past regarding the component of oblique motion on the fault. Cunningham (2001) described the fault as right-lateral oblique and Baljinnyam et al. (1993) described it as left-lateral oblique. Slickenline data indicate that there is a component of right-lateral slip, assuming the fault also has a normal slip component. There is no evidence of laterally displaced features on the modern earthquake scarp because the scale of the offset is so small.

The relationship between earthquake magnitude and rupture geometries implies that the Egiin Davaa fault ruptured in a large, ~M7.3 earthquake. This earthquake most likely ruptured the 51-km long southwestern strand of the fault, however it may have ruptured across a segment boundary for a total rupture length of 70 km.

REFERENCES

Avouac, J-P, 1993, Analysis of scarp profiles: Evaluation of errors in morphologic dating: Journal of Geophysical Research, v. 98, p. 6745-6754.

Baljinnyam, I., Bayasgalan, A., Borisov, B., Cisternas, A., Dem'yanovich, M.G., Ganbaatar, L., Kochetkov, V.M., Kurushin, R.A., Molnar, P., Phillip, H., and Vashchilov, Y.Y., 1993, Ruptures of major earthquakes and active deformation in Mongolia and its surroundings:

Geological Society America Memoir 181.

Bayasgalan, A., Jackson, J., and McKenzie, D., 2005, Lithoshpere rheology and active tectonics in Mongolia: Relations between earthquake source parameters, gravity and GPS measurements: Geophysical Journal International, v.163, p. 1151-1179.

Calais, E., Vergnolle, M., Sankov, V., Lukhnev, A., Miroshnitchenko, A., Amarjargal, S., and Deverchere, J., 2003, GPS measurements of crustal deformation in the Baikal-Mongolia area (1994-2002): Implications for current Kinematics of Asia: Journal of Geophysical Research, v. 108, no. B10, p. 2501.

Colman, S. M., and Watson, K., 1983, Ages estimated from a diffusion equation model for scarp degradation: Science, v. 221, p. 263–265.

Cunningham, W.D., 2001, Cenozoic normal faulting and regional doming in the southern Hangay region, Central Mongolia: Implications for the origin of the Baikal rift province: Tectonophysics, v. 331, p. 389-441.

Hanks, T.C., 2000, The age of scarplike landforms from diffusion-equation analysis, *in* Noller, J.S., Sowers, J.M. and Lettis, W.R., eds., Quaternary Geochronology: Methods and Applications, AGU, Washington, D.C., p. 313–338.

Khilko, S.D., Kurushin, R.A., Kochetkov, V.M., Balzhinnyam, I., and Monkoo, D., 1985, Strong Earthquakes, paleoseismogeological and macroseismic data, in Earthquakes and the bases for Seismic zoning of Mongolia, Transactions 41: The Joint Soviet-Mongolian Scientific Geological Research Expedition: Moscow, Nauka, p.19-83.

Stuiver, M., and Polach, H., 1977, Discussion: Reporting of 14C Data: Radiocarbon 19, no.3, p. 355-363.

Tapponnier, P., and Molnar, P., 1979, Active faulting and Cenozoic tectonics of the Tien Shan, Mongolia, and Baykal regions: Journal of Geophysical Research, v. 84, p. 3425-3459.

Wells, D. L., and Coppersmith, K. J., 1994, New empirical relationships among magnitude, rupture length, rupture width, rupture area, and surface displacement: Bulletin of the Seismological Society of America, v. 84, no. 4, p. 974-1002.

Yeats, R. S., Sieh, K., and Allen, C.R., 1997, The Geology of Earthquakes: New York, Oxford University Press.